Cell response to substrate rigidity is regulated by active and passive cytoskeletal stress

Bryant L. Doss[a,1], Meng Pan[a,1], Mukund Gupta[a,b], Gianluca Grenci[a,c], René-Marc Mège[b], Chwee Teck Lim[a,c,d], Michael P. Sheetz[a,e], Raphaël Voituriez[f,g], and Benoît Ladoux[b,2]

[a]Mechanobiology Institute, National University of Singapore, Singapore 117411; [b]Université de Paris, CNRS, Institut Jacques Monod, 75013 Paris, France; [c]Department of Biomedical Engineering, National University of Singapore, Singapore 117583; [d]Institute for Health Innovation & Technology (iHealthtech), National University of Singapore, Singapore 117599; [e]Molecular Mechanomedicine Program and Department of Biochemistry and Molecular Biology, University of Texas Medical Branch, Galveston, TX 77555; [f]Laboratoire de Physique Théorique de la Matière Condensée, CNRS/Sorbonne University, F-75005 Paris, France; and [g]Laboratoire Jean Perrin, CNRS/Sorbonne University, F-75005 Paris, France

Edited by David A. Weitz, Harvard University, Cambridge, MA, and approved April 22, 2020 (received for review October 9, 2019)

Morphogenesis, tumor formation, and wound healing are regulated by tissue rigidity. Focal adhesion behavior is locally regulated by stiffness; however, how cells globally adapt, detect, and respond to rigidity remains unknown. Here, we studied the interplay between the rheological properties of the cytoskeleton and matrix rigidity. We seeded fibroblasts onto flexible microfabricated pillar arrays with varying stiffness and simultaneously measured the cytoskeleton organization, traction forces, and cell-rigidity responses at both the adhesion and cell scale. Cells adopted a rigidity-dependent phenotype whereby the actin cytoskeleton polarized on stiff substrates but not on soft. We further showed a crucial role of active and passive cross-linkers in rigidity-sensing responses. By reducing myosin II activity or knocking down α-actinin, we found that both promoted cell polarization on soft substrates, whereas α-actinin overexpression prevented polarization on stiff substrates. Atomic force microscopy indentation experiments showed that this polarization response correlated with cell stiffness, whereby cell stiffness decreased when active or passive cross-linking was reduced and softer cells polarized on softer matrices. Theoretical modeling of the actin network as an active gel suggests that adaptation to matrix rigidity is controlled by internal mechanical properties of the cytoskeleton and puts forward a universal scaling between nematic order of the actin cytoskeleton and the substrate-to-cell elastic modulus ratio. Altogether, our study demonstrates the implication of cell-scale mechanosensing through the internal stress within the actomyosin cytoskeleton and its coupling with local rigidity sensing at focal adhesions in the regulation of cell shape changes and polarity.

mechanobiology | cytoskeleton | rigidity sensing | cell polarity

As opposed to passive materials, cells actively respond to mechanical perturbations occurring in their surrounding environment including external forces (1, 2), substrate stiffness (3, 4), and geometry (5, 6). In this context, substrate stiffness has been shown to play a major role in cell mechanosensitivity and cell phenotype (7). Observable phenotypic changes for single cells cultured on soft or stiff substrates include focal adhesion and cell area (8), traction stresses (3, 9, 10), actin cytoskeleton organization (11–13), and cell differentiation (4). Notably, cells are unable to establish front-rear polarity and form ventral stress fibers on soft substrates. Actomyosin is utilized by cells to sense substrate rigidity at the scale of a single adhesion with contraction-response cycles, and several molecular mechanisms using this have been described (14–17). Those sensing events are brief (<1 min) but influence the lifetime of adhesions and contractility, and cumulatively after long times and many sensing events (several hours), cells adopt a quasi-steady state configuration that reflects both adhesion behavior and cell-scale mechanosensitivity mediated through actomyosin (18). However, the integration of these in regulating tissue- and cell-scale behavior is not well understood.

The cell's actomyosin network is mechanoresponsive and can adapt its rheological parameters such as stiffness, viscosity, and myosin activity to environment mechanical cues (19–21) that are largely sensed through adhesions. As cells must undergo a symmetry breaking process to establish front-rear polarity in which physical forces play a key role (22), we hypothesized that a cell's ability to polarize and adapt to environmental mechanical cues is influenced by the interplay and coupling between the physical properties intrinsic to the actin cytoskeleton, adhesions established by local rigidity sensing contractions, and the substrate.

Proteins contributing to the mechanical properties of an actin network include active cross-linkers (myosin) and passive cross-linkers (including α-actinin [ACTN], filamin, fascin, and others). In vitro rheological studies on actin gels show a power-law type relationship between elastic modulus and cross-linker concentration (23) which depends on the specific binding affinity between the cross-linker and actin (24), the strain rate (25), and the prestress (26). Global actomyosin contraction dynamics are directly regulated by the amount of ACTN cross-linking in an actin gel (27) and lack of ACTN has been also shown to disrupt actin network symmetry in vitro and in cells (28). Here, we describe a functional role of myosin II and ACTN cross-linking in preserving cell symmetry, regulating cell-scale ordering of the cytoskeleton, and tuning the cytoskeleton's adaptive response to substrate rigidity that reflects changes in adhesions incurred via local rigidity sensing. Both molecules contribute to determine

Significance

The observation that cells sense and adapt to the physical stiffness of their environment is consistent across many different cell types and has profound implications in the final biological phenotype. In a diseased state or transformed cell, the substrate rigidity sensing and adaptation machinery is perturbed or outright abolished, which leads to progression of the disease, thus fully understanding this process is vital. Here, we found that the organization of the actin cytoskeleton in fibroblasts was governed by active and passive cross-linkers and the relative cell-to-substrate elasticity, and we present a phenomenological model detailing this. As cell rigidity sensing is a robust mechanism observed in various contexts, a generalized physics-based understanding such as presented here will yield universal insights.

Author contributions: R.V. and B.L. designed research; B.L.D. and M.P. performed research; B.L.D., M.P., M.G., G.G., R.-M.M., C.T.L., R.V., and B.L. contributed new reagents/analytic tools; B.L.D., M.P., R.-M.M., M.P.S., R.V., and B.L. analyzed data; and B.L.D., R.V., and B.L. wrote the paper.

The authors declare no competing interest.

This article is a PNAS Direct Submission.

Published under the PNAS license.

[1]B.L.D. and M.P. contributed equally to this work.

[2]To whom correspondence may be addressed. Email: benoit.ladoux@ijm.fr.

This article contains supporting information online at https://www.pnas.org/lookup/suppl/doi:10.1073/pnas.1917555117/-/DCSupplemental.

First published May 22, 2020.

the active and passive rheological properties of the actomyosin cytoskeleton, and cell polarity will only be established when the active stress is above a critical threshold and the substrate stiffness is higher than that of the cell.

Results

Actin Organization and Composition Is Rigidity Dependent. We used a microfabricated array of flexible polydimethylsiloxane (PDMS) pillars to measure the traction forces exerted by the cell while simultaneously observing the organization of the actin cytoskeleton (Fig. 1*A*). By tuning the height of the pillar, we also changed the stiffness of the pillar (in a cantilever bending definition) while maintaining constant Young's modulus (~2 MPa) of the PDMS and similar diameter (~2 μm) (*SI Appendix*, Fig. S1*A*). The top surface of the pillar substrate was coated with fibronectin via microcontact printing, and the sidewalls were passivated (*Materials and Methods*) such that cells only attached to the pillar tops. We seeded wild-type REF52 (REF52-WT) fibroblasts onto pillar substrates with stiffness 4 nN/μm and 55 nN/μm for 5 h and performed immunostaining to observe the actin organization (Fig. 1*B*) and protein localization (Fig. 1*C*). Consistent with previous studies (12, 13), on soft pillars, actin organized into a system of radial and transverse fibers with circular symmetry; on stiff pillars, it globally aligned into polarized, ventral stress fibers.

On soft substrates, ACTN4 concentrated along short radial fibers nearby focal adhesions and, to a lesser extent, along the transverse fibers (Fig. 1*C*), whereas myosin IIA only concentrated along transverse fibers. This was similar to fibroblasts spreading into circular patterns at early times (22). On stiff substrates, both myosin IIA and ACTN4 localized along ventral stress fibers (Fig. 1*B*), consistent with other studies (29). While ACTN binds integrin and has been shown to play a role in focal adhesions (30), we observed that the peak ACTN intensity was roughly 1 μm toward the adhesion proximal end from the peak intensity of paxillin and fibronectin (*SI Appendix*, Fig. S1*B*). As both the organization of actin as well as the localization of myosin IIA and ACTN4 changed as a function of substrate stiffness, we questioned whether these proteins that relocated during polarization were also mechanistically involved in rigidity sensing.

Reducing Myosin Activity Promotes Polarization on Soft Substrates. To perform live cell experiments and facilitate simultaneous monitoring of both actin organization and cell traction forces, we generated a REF52 line stably expressing tdTomato-F-tractin (REF52-Ftractin), an f-actin reporter (31). We seeded the cells

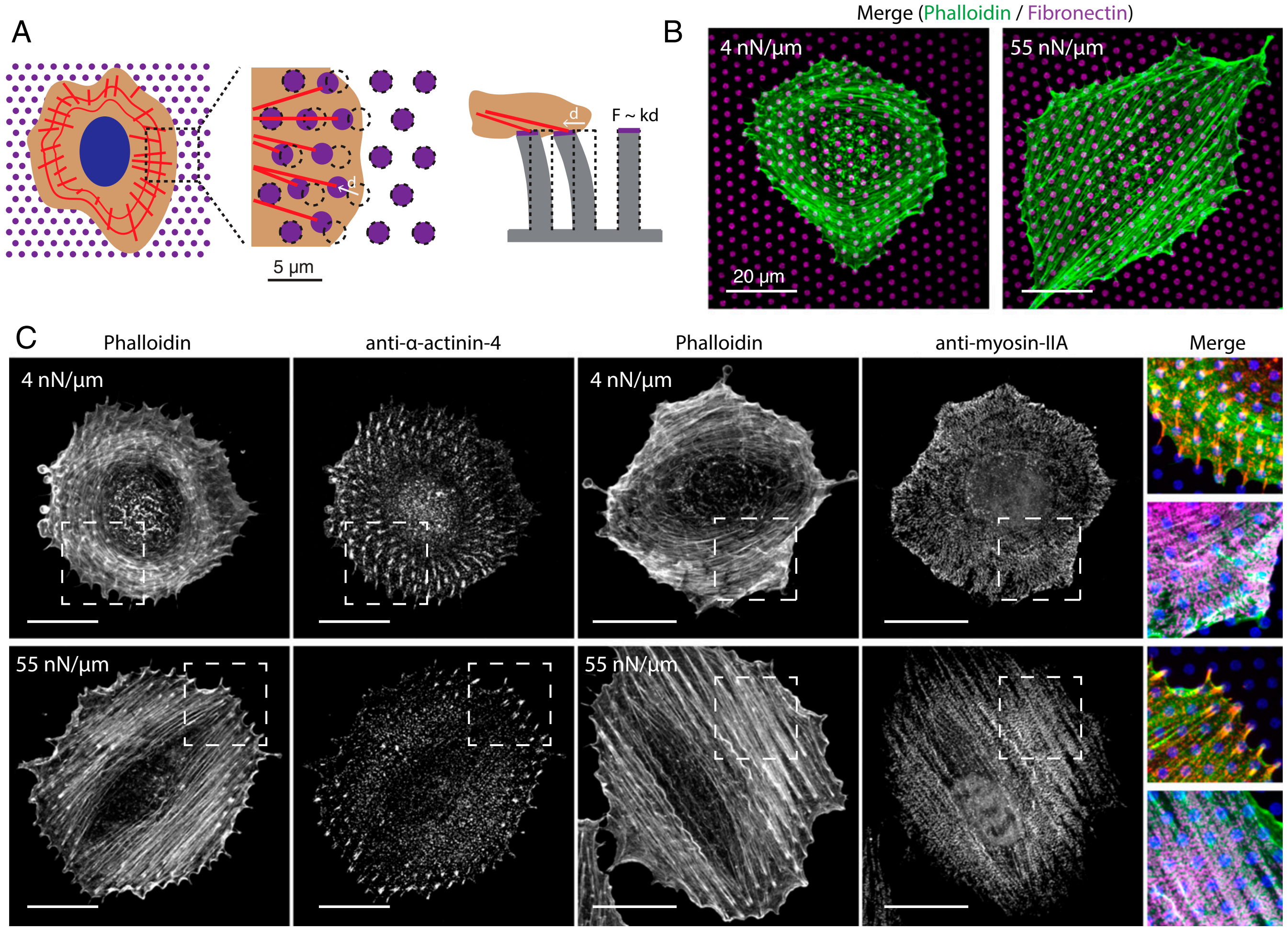

Fig. 1. REF52 fibroblasts exhibit differential actin ordering and actin–cross-linking protein localization on soft and stiff substrates. (*A*) Schematic of micropillar experiments showing actin (red) and fibronectin (magenta). (*B*) Confocal fluorescence images (maximum intensity projection) of REF52-WT fibroblasts seeded onto soft (*Left*) and stiff (*Right*) micropillar substrates coated with fibronectin (magenta) and stained for phalloidin (green). (*C*) Confocal fluorescence images (maximum intensity projection) of REF52-WT fibroblasts seeded onto soft (*Upper*) and stiff (*Lower*) micropillar substrates and stained with phalloidin, anti–α-actinin-4, anti-myosin IIA, and fibronectin, and zoomed and merged images (*Right*: blue, fibronectin; green, phalloidin; magenta, anti-myosin IIA; red, anti-ACTN4). (Scale bars, 20 μm.)

onto soft and stiff pillars and quantified the organization of the actin cytoskeleton at the cell scale by the nematic order parameter (10, 13) (Fig. 2*A*), which is zero when actin is isotropic or circular and one when actin is polarized along a single axis (*Materials and Methods*), and the cellular traction forces (Fig. 2*B*).

We treated cells with varying concentrations of blebbistatin to test the effect of myosin II on polarization and traction force generation (Fig. 2 *C*–*E*). Cells treated with high concentrations (>20 μM) displayed markedly reduced traction stresses and a disorganized actin network on both pillar stiffnesses, while cells treated with very low concentrations (<1 μM) exhibited similar rigidity-dependent ordering of actin and traction stress patterns as in untreated cells. Surprisingly, at intermediate concentrations (2.5–10 μM), traction stresses were moderately attenuated and cells on soft pillars formed ventral stress fibers and polarized. While it was counterintuitive that reducing myosin II activity promoted ventral stress fiber formation, Oakes et al. observed stress fiber formation despite large (~75%) reductions in cytoskeletal tension (32). Cells treated with 5 μM blebbistatin retained stress fibers and localization of both ACTN4 and myosin IIA to the cell lamella (*SI Appendix*, Fig. S2 *A* and *B*). Cells on soft pillars treated with varying amounts of the Rho-associated protein kinase (ROCK) inhibitor Y-27632 behaved similarly (*SI Appendix*, Fig. S2 *C* and *D*); traction force magnitudes inversely scaled with Y-27632 concentration, at intermediate concentrations actin organized into ventral stress fibers with global alignment, and actin organization was lost at high concentrations. Furthermore, treating cells with either nocodazole or calyculin A to increase contractility resulted in lower nematic ordering on both soft and stiff substrates (*SI Appendix*, Fig. S2 *E* and *F*).

The morphology of the cells was also affected by treatment with blebbistatin, with intermediately treated cells having higher area and aspect ratio (*SI Appendix*, Fig. S3 *A*–*D*). To test if increasing cell area directly caused the enhanced nematic ordering in myosin-inhibited cells, we seeded cells onto pillars stamped with fibronectin in circular (diameter = 60 μm) and teardrop patterns to confine the cell (*SI Appendix*, Fig. S3 *E*–*G*). On soft pillars, untreated cells displayed the usual system of circular transverse arcs and radial stress fibers, and cells treated with 5 μM blebbistatin had globally aligned ventral stress fibers. Therefore, we concluded that actin organization in myosin II-inhibited cells on various pillars stiffnesses was a consequence of cytoskeletal properties rather than solely cell shape changes, which has been previously explored (33).

The maximum traction force on a single soft pillar was lower than that on stiff pillars, although the traction forces on soft pillars

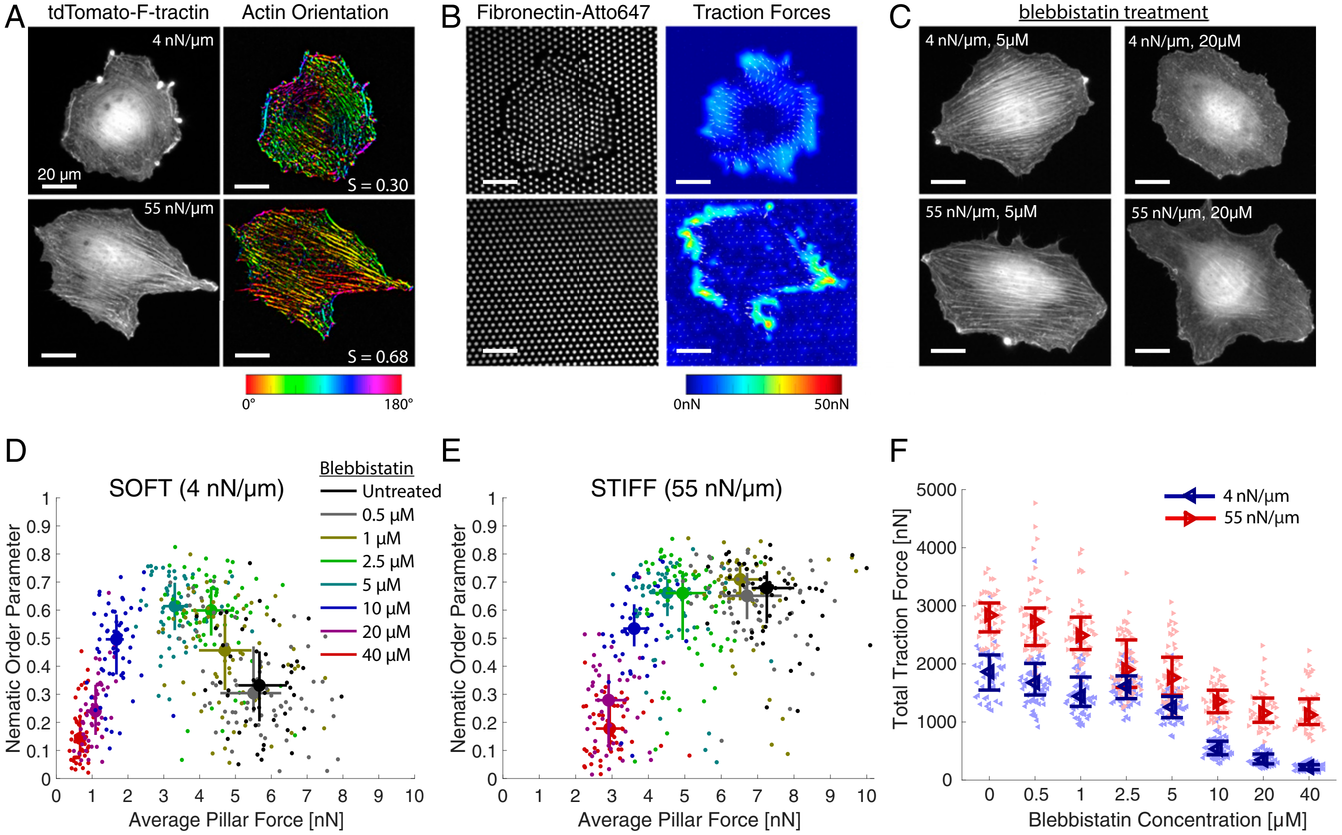

Fig. 2. Inhibiting myosin II tunes actin cytoskeleton ordering on different substrate stiffnesses. (*A*) (*Left*) Widefield fluorescence images of live REF52-Ftractin cells showing tdTomato-F-tractin for soft (*Upper Left*) and stiff (*Lower Left*), and (*Right*) the local angle of actin and nematic order parameter quantification for soft (*Upper Right*) and stiff (*Lower Right*). (*B*) (*Left*) Widefield fluorescence images of fibronectin-Atto647N on the pillar tops for soft (*Upper Left*) and stiff (*Lower Left*), and quantification of the cell traction force vectors and magnitudes for soft (*Upper Right*) and stiff (*Lower Right*). (*C*) Widefield fluorescence images showing tdTomato-F-tractin of REF52-Ftractin cells on different pillar stiffnesses and treated with varying amounts of blebbistatin. (*D*) Scatterplots showing quantification of nematic order parameter versus average traction stress on soft pillars with different concentrations of blebbistatin. Circles and error bars indicate median ± interquartile range. (*E*) Scatterplots showing quantification of nematic order parameter versus average traction stress on stiff pillars with different concentrations of blebbistatin. Circles and error bars indicate median ± interquartile range. (*F*) Total traction force exerted by cells with varying concentration of blebbistatin on soft and stiff pillars. Markers with error bars indicate median ± interquartile range. (*D*–*F*) Soft pillars *n* = 46, 71, 66, 64, 58, 61, 49, 48 cells, stiff pillars *n* = 51, 60, 50, 64, 60, 47, 45, 49 cells for untreated, 0.5 μM, 1 μM, 2.5 μM, 5 μM, 10 μM, 20 μM, and 40 μM blebbistatin, respectively. Data in *D*–*F* are merged from two independent experiments per condition. For high concentrations of blebbistatin on stiff pillars in *E* and *F*, traction force measurements were limited by the system detection resolution. (Scale bars, 20 μm.)

were broadly distributed under the cell and along the entire perimeter, whereas the traction forces on stiff pillars condensed onto a subset of pillars at the cell edge on its long axis. We quantified the total traction force exerted by the cell (*Materials and Methods*) and observed that the total traction force on stiff pillars was about 50% higher than on soft (2.8 ± 0.3 vs. 1.9 ± 0.3 μN for untreated cells on stiff and soft, respectively) (Fig. 2*F*). Thus, cells were able to deflect a larger amount of soft pillars to a larger distance than stiff pillars to achieve a similar order of magnitude of traction force despite the pillar stiffness being drastically different, which indicated a coupling of both adhesion- and cell-scale mechanosensitivity.

Rigidity-Dependent Cell Polarization Is Tuned by Passive ACTN Cross-linking. We saw a strong correlation between traction stresses and alignment of actin filaments, whereby actin aligned at high traction stresses on stiff substrates (Fig. 2*E*); however, on soft substrates, actin only globally aligned at intermediate traction stresses (Fig. 2*D*). As myosin was inhibited, the active stress in the actin network decreased and its passive rheological response was

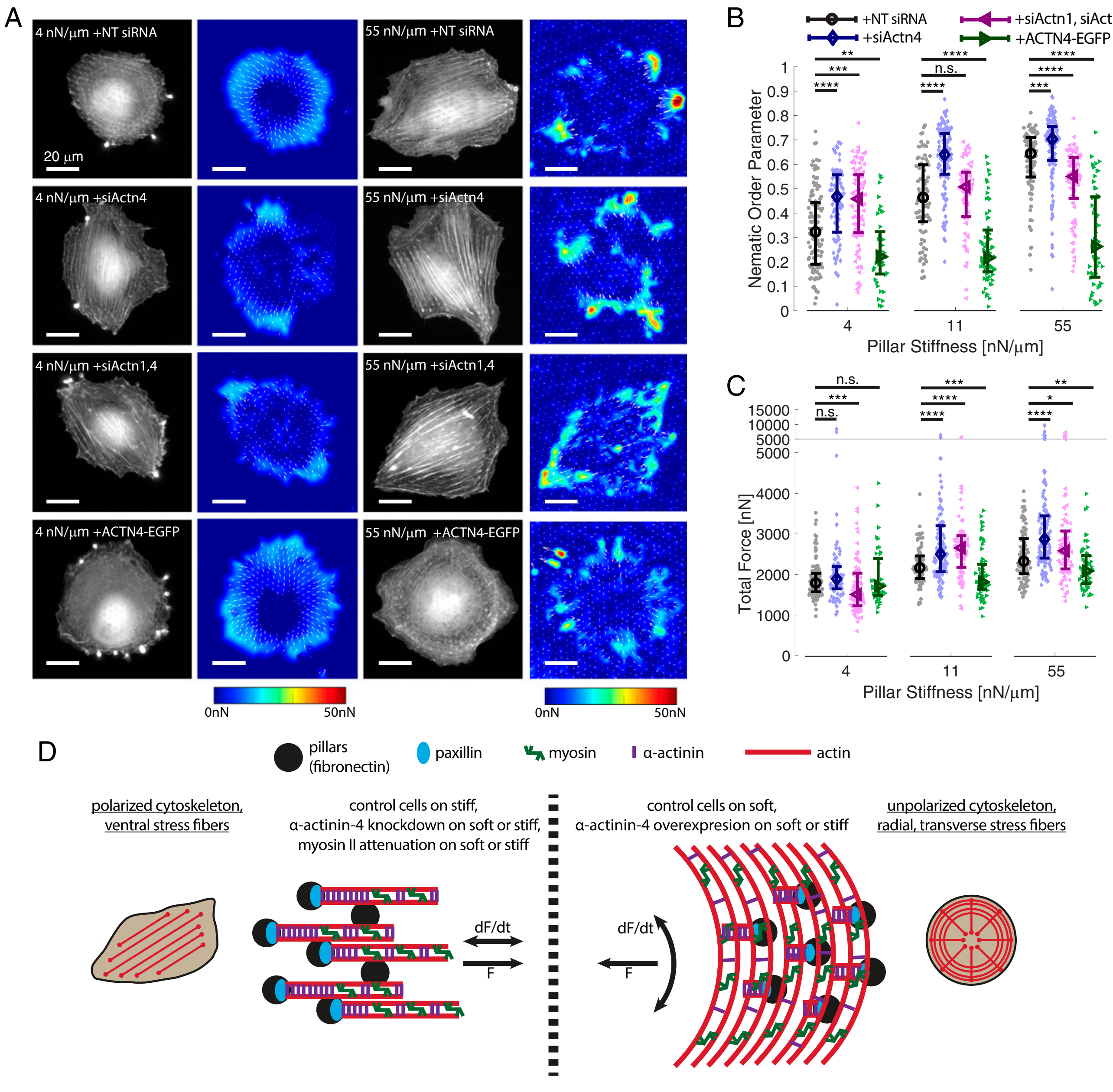

Fig. 3. Inhibiting passive ACTN cross-linking affects cell rigidity sensing. (*A*) Widefield fluorescence images of live REF52-Ftractin cells showing tdTomato-F-tractin on soft and stiff pillars and traction force maps for different amounts of ACTN cross-linking. (*B*) Quantification of the nematic order parameter for different ACTN expression and different substrate stiffnesses. Markers with error bars indicate median ± interquartile range. (*C*) Quantification of the total traction force for different ACTN expression treatments and different substrate stiffnesses. Markers with error bars indicate median ± interquartile range. (*B* and *C*) +NT siRNA n = 112, 84, 91 cells for k = 4 nN/μm, 11 nN/μm, 55 nN/μm, respectively; +siActn4 n = 81, 110, 130 cells for k = 4 nN/μm, 11 nN/μm, 55 nN/μm, respectively; +siActn1,4 n = 96, 70, 83 cells for k = 4 nN/μm, 11 nN/μm, 55 nN/μm, respectively; +ACTN4-EGFP n = 40, 65, 53 cells for k = 4 nN/μm, 11 nN/μm, 55 nN/μm, respectively. Data in *B* and *C* are merged from at least two independent experiments per condition. (Scale bars, 20 μm.) P values were calculated using Mann–Whitney U test, not significant (n.s.) $P > 0.05$, *$P < 0.05$, **$P < 0.01$, ***$P < 0.001$, ****$P < 0.0001$. (*D*) Summary cartoon showing the organization of the actin cytoskeleton on stiff (*Left*) and soft (substrates) (*Right*) under different conditions tested in this work.

modified as well. Because the global mechanical response of cells was controlled by the coupled action of active and passive cross-linkers (34), we sought to disentangle such effects and examine the role of passive cross-linking in rigidity sensing.

We tuned the amounts of passive ACTN cross-linking by small interfering RNA (siRNA)-mediated knockdowns of ACTN1, ACTN4, or both ACTN1 and ACTN4 simultaneously (pan-ACTN), or by transient overexpression of ACTN1-EGFP or ACTN4-EGFP (*SI Appendix*, Fig. S4 *A–C*). As a control, cells transfected with nontargeting (NT) siRNA exhibited a rigidity-dependent propensity to polarize (Fig. 3 *A* and *B*) and spatial organization of traction forces. Cells with ACTN4 or pan-ACTN knockdown formed bundled ventral stress fibers, consistent with other studies (29, 35, 36), and had increased nematic organization of actin on soft substrates. The pan-ACTN knockdown resulted in stress fibers that had less global ordering than ACTN4 knockdown or control cells on stiff substrates. Cells overexpressing ACTN4-EGFP preserved a system of radial and transverse actin fibers and had reduced nematic ordering on all substrates. In addition, the actin network was more uniformly dense with few bundles. Knockdown of only ACTN1 did not affect rigidity sensing or actin bundling; however, overexpressing ACTN1-EGFP had a similar phenotype as overexpressing ACTN4-EGFP (*SI Appendix*, Fig. S4 *D* and *E*). Furthermore, we overexpressed ACTN1-ABDdel-EGFP (30), a dominant-negative mutant in which the actin binding domain is deleted but will still form dimers with endogenous ACTN (both ACTN1 and ACTN4; ref. 37) to inhibit cross-linking (*SI Appendix*, Fig. S4 *D* and *E*). This resulted in a phenotype similar to the pan-ACTN knockdown whereby ventral stress fibers formed on all stiffness, had increased ordering compared to control cells on soft substrates, and decreased ordering on stiff substrates. The ACTN4 knockdown phenotype was rescued by overexpression of either ACTN1-EGFP or ACTN4-EGFP, and we observed a strong negative correlation between ACTN expression level and nematic order parameter (*SI Appendix*, Fig. S5), which also accounted for cell-to-cell variability in protein overexpression amount. Morphologically, the aspect ratio of the cell shape exhibited a similar trend as the actin nematic order parameter (*SI Appendix*, Fig. S4*F*). Therefore, we concluded that actin organization was regulated by ACTN and that an optimal amount of cross-linking promoted polarization on various substrate stiffnesses; too much cross-linking resulted in unpolarized cells on all stiffness and too little resulted in isotropic actin networks, with cells on soft substrates requiring less ACTN cross-linking to polarize.

Altering ACTN cross-linking also perturbed the magnitude and spatial patterns of traction forces (Fig. 3 *A* and *C*). Consistent with other studies (35, 38), the total traction force exerted by the cell was highest in ACTN4 knockdown (Fig. 3*C*). On soft substrates, the order parameter of the traction force vectors was higher for ACTN4 or pan-ACTN knockdown cells, whereas it was lowest on all substrates with ACTN4-EGFP overexpressing cells (*SI Appendix*, Fig. S4*G*). Both the amount of cell traction forces pointing toward the cell center of mass (*SI Appendix*, Fig. S4*H*) as well as the spatial correlation of traction force vectors (*SI Appendix*, Fig. S4*I*) was highest in ACTN4-EGFP overexpressing cells and decreased as ACTN cross-linking was reduced, which implied that the spatial symmetry of traction forces was controlled by ACTN concentration, in line with another study (28).

We next performed time lapse imaging of the cells to observe the dynamics of traction forces and actin (Movies S1–S4). As previously observed (13), control cells on soft pillars had a combined system of radial and transverse fibers that flowed inwards from the cell boundary. In contrast, cells on stiff pillars formed ventral stress fibers that were stable throughout a 40-min imaging window (*SI Appendix*, Fig. S6 *A–C*). We observed that the force fluctuation magnitude was higher in pan-ACTN knockdown cells compared to control (*SI Appendix*, Fig. S6*D*). While static traction forces were radially directed toward the center of mass, we observed that the direction of the dynamic traction forces on soft pillars was more orthoradial (*SI Appendix*, Fig. S6*F*). On stiff substrates, control cells formed ventral stress fibers and the traction forces fluctuated in the same direction as the static forces (*SI Appendix*, Fig. S6*E*). In pan-ACTN knockdown cells, the stability of ventral stress fibers that formed on soft pillars was similar to those on stiff and the dynamic forces fluctuated along the same direction as the static (*SI Appendix*, Fig. S6 *A* and *F*).

Our experimental results of actin organization on micropillars are summarized in Fig. 3*D*. When the substrate is soft, or ACTN is overexpressed, cells retain a circular shape with a combination of radial and transverse fibers that flow inward and myosin motors indirectly develop traction forces. When the substrate stiffness is high, ACTN4 is knocked down, or myosin II is inhibited with small concentrations of blebbistatin, then circular symmetry is broken, ventral stress fibers form, and the cytoskeleton is more polarized. When the ACTN cross-linking is highly attenuated (pan-ACTN knockdown or ACTN1-ABDdel overexpression), or contractile activity is depleted by a large concentration of blebbistatin, then the cytoskeleton is more isotropic, although ACTN depletion promotes ventral stress fiber formation and large concentrations of blebbistatin abolish stress fiber formation.

Cytoskeletal Stiffness Correlates with ACTN Concentration and Myosin II Activity. We observed increased actin ordering at an optimal amount of either myosin II activity or ACTN cross-linking. However, the magnitude of traction stress at which order arose on a given stiffness was not the same in the two scenarios as blebbistatin treatment reduced traction forces while ACTN knockdown increased traction forces. We next considered how myosin II and ACTN affected the rheology of the cell; the elasticity of a single cell correlates with traction force (39) and for an actin network scales with cross-linker concentration (23). As both passive and active cross-linking contribute to cell rheological properties, we considered that the ordering of the cytoskeleton might be more generally governed by the actin network stiffness.

We seeded cells onto plastic dishes and performed atomic force microscopy (AFM) nanoindentation (Fig. 4*A* and *SI Appendix*, Fig. S7) in a rapid force-volume scanning mode with high lateral resolution (*Materials and Methods*) and with different conditions of ACTN knockdown (ACTN4, pan-ACTN, NT control), overexpression (ACTN4-EGFP), and cells treated with 5 μM blebbistatin. The local elastic modulus in the cytoskeleton strongly depended on the precise location probed; points on a stress fiber were about an order of magnitude stiffer than indentation points between the stress fibers (*SI Appendix*, Fig. S7*D*). Further, by correlating the local elastic modulus with the local height, we observed that very thin lamellipodial and thick nuclear regions were both softer than the lamella region (*SI Appendix*, Fig. S7*E*). We found that ACTN4-EGFP overexpression resulted in the stiffest lamella (here defined as locations with height <2 μm), followed by control, ACTN4 knockdown, and pan-ACTN knockdown, indicating that the mean lamella stiffness positively correlated with ACTN concentration (Fig. 4 *B* and *C*). By scanning we resolved the stiffness of stress fibers within a cell (Fig. 4*D*) and found that the stress fiber stiffness decreased with blebbistatin treatment. As the protein localization of ACTN4 and myosin IIA remained on stress fibers after blebbistatin treatment (*SI Appendix*, Fig. S2 *A* and *B*), we attributed this stiffness decrease to a loss of contractility. Cells with ACTN4 knockdown had stress fibers with similar stiffness as control; however, there were more soft regions between the fibers as they became more bundled. Cells with ACTN4-EGFP overexpression were unpolarized and exhibited the stiffest lamella; however, the nuclear region of these cells was softer than in the other conditions, which may have been indicative of a defect in the perinuclear actin cap which control cells could form.

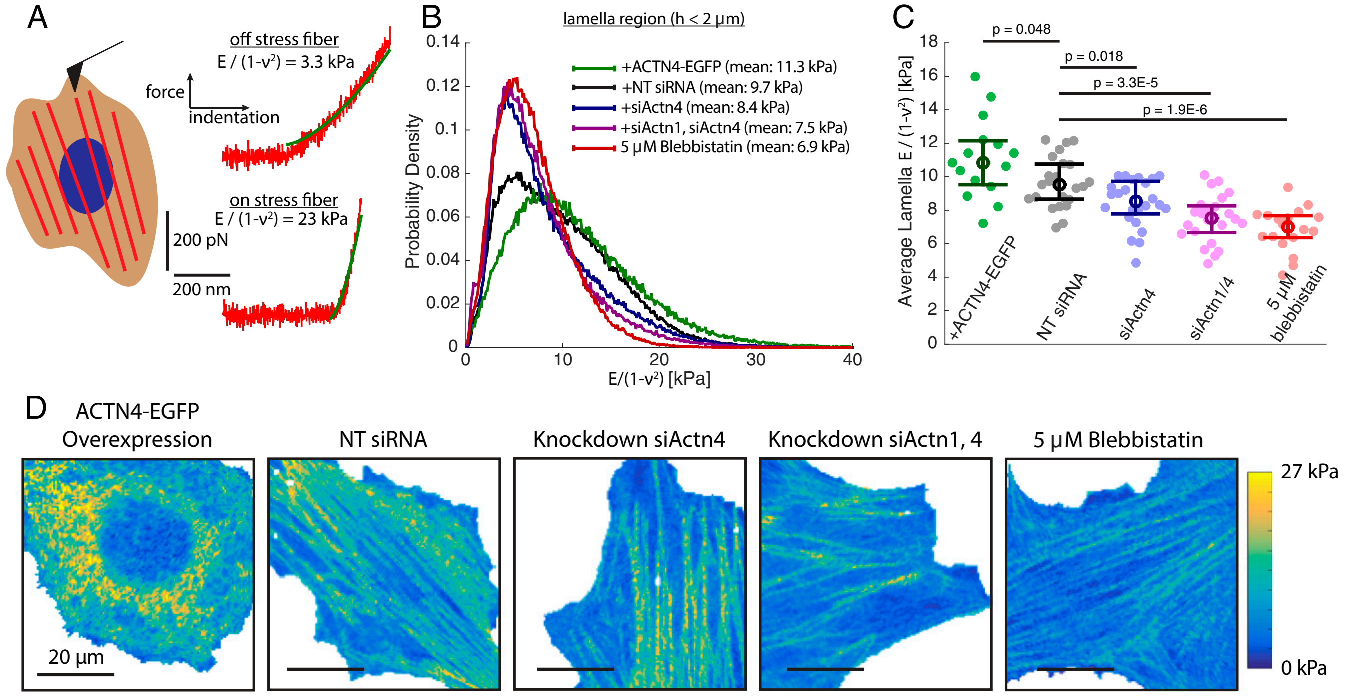

Fig. 4. Inhibiting myosin II or reducing ACTN cross-linking softens the cytoskeleton. (*A*) Schematic of the AFM experiment showing representative force-indentation curves and fits on a stress fiber region (*Lower Right*) and outside of a stress fiber (*Upper Right*). (*B*) Probability density (normalized histogram) of force-indentation curves with mean elastic modulus in the cell lamella region (h < 2 µm) for REF52-Ftractin cells with ACTN4-EGFP overexpression, NT siRNA control, ACTN4 knockdown, pan-ACTN knockdown, and 5 µM blebbistatin. (*C*) Comparison of mean elastic modulus for a given cell in the lamella region between the conditions. Markers with error bars indicate median ± interquartile range. *P* values were calculated using Mann–Whitney *U* test. Dataset *B* and *C* is $n = 15, 24, 24, 24, 18$ cells and $n = 138{,}201, 237{,}045, 227{,}187, 220{,}154, 170{,}595$ curves for +ACTN4-EGFP, +NT siRNA, +siActn4, +siActn1,4, 5 µM blebbistatin, respectively; data were combined from at least two independent experiments per condition. (*D*) Maps of the elastic modulus for REF52-Ftractin cells with (left to right) ACTN4-EGFP overexpression, NT siRNA control, ACTN4 knockdown, pan-ACTN knockdown, and 5 µM blebbistatin. The color indicates the fitted $E/(1-\upsilon^2)$ at each pixel. (Scale bars, 20 µm.)

Cytoskeleton Elasticity and Activity Regulate Rigidity-Dependent Ordering. Control cells on soft substrates or cells with ACTN overexpression appeared to be incapable of undergoing a symmetry breaking process which cells must first undergo to establish polarity, whereas control cells on stiff substrates, ACTN knockdown cells, or cells with intermediate myosin II inhibition had broken symmetry. This behavior can be recapitulated in a phenomenological physical model, whose main ingredients are summarized below (see *SI Appendix* for details). The model provides a minimal coarse grained description of the actin cytoskeleton of a cell seeded on a surface as a two-dimensional layer of active gel that can undergo an isotropic to nematic transition upon increasing actin filament density ρ, analogous to that of lyotropic liquid crystals (13, 40). We adopt the simplest mean-field description where variables are assumed to be uniform in space. The alignment of actin filaments can then be quantified by the cell-averaged nematic order parameter *S*, which satisfies close to the isotropic-nematic transition:

$$S \propto (\rho - \rho_c)^{\frac{1}{2}}\,, \qquad [1]$$

for $\rho > \rho_c$ while $S = 0$ for $\rho < \rho_c$, where $\propto$ denotes proportionality and ρ_c is the critical actin density required for symmetry breaking. Qualitatively, this yields a negligible actin ordering at low density ($\rho < \rho_c$) and an increasing ordering with density for $\rho > \rho_c$. We assume below that cells remain close to the isotropic-nematic transition. As opposed to classical equilibrium systems, the model assumes that the filament density is actively regulated by the total averaged stress σ^s at the cell-substrate interface. To linear order in σ^s (limit of low activity), this can be written $\rho = \rho_0 + \chi \mathrm{Tr}(\sigma^s)$, where $\chi > 0$ is a phenomenological coupling constant that encodes the mechanosensitive response to stress and ρ_0 is a reference density in absence of stress; under this hypothesis, the mean actin filament density increases when the pulling stress increases at the cell-substrate interface. This is qualitatively supported at the level of focal adhesions, which are expected to mediate such mechanosensitive response; fluorescence recovery after photobleaching of GFP-talin showed an increased stability of focal adhesions on stiff pillars or with higher pillar traction force compared to soft pillars or lower traction forces (*SI Appendix*, Fig. S8 and Movie S5), thus the stability of focal adhesions and, hence, actin filament density, was indeed gated by local force.

In the cell, the stress can be decomposed into a passive component σ^e and an active component σ^a. The passive stress is assumed to be of elastic nature and controlled mainly by the elastic modulus E_c of the actin network. Here, we assume for the sake of simplicity a classical isotropic elastic response (independent of ρ in the limit of low activity), which is expected to hold close to the isotropic-nematic transition. The cytoskeleton is described at a coarse-grained level as a uniform material, E_c is therefore the effective cell-scale stiffness, which is likely to be controlled at the microscopic scale by the local actin organization (stress fibers or cortex). σ^a is induced by myosin contractility, which is parametrized by the phenomenological constant ζ_0; the isotropic component of σ^a is then set by ρ and ζ_0 according to $\sigma^a_{ij} = \zeta_0 \rho \delta_{ij}$. Continuity of stress at the cell-substrate interface can then be written $\sigma^e + \sigma^a = \sigma^s$. After taking the trace and averaging over the cell contour it follows that

$$\frac{\rho}{\rho_0} = \frac{E_s + CE_c}{E_s(1 - 2\chi\zeta_0) + CE_c} \equiv f\left(\frac{E_s}{E_c}\right), \qquad [2]$$

where E_s is the Young's modulus of the substrate, assumed elastic (the pillar substrate Poisson's ratio ν_s is assumed to be zero for simplicity), and C is a dimensionless constant that depends on cell shape and Poisson's ratio. This equation defines the scaling function f that depends on E_s and E_c only via E_s/E_c; note however that f is not universal since it depends on the cell shape and Poisson's ratio. The main prediction of this simple model is hence that the density and nematic organization of actin are critically controlled by the elastic modulus of the substrate relative to that of the cell E_s/E_c (*SI Appendix*, Fig. S9) and that the critical substrate stiffness k* (E_s when $\rho = \rho_c$) required for the cell to break symmetry is determined by the stiffness of the actin cytoskeleton, as was experimentally observed. Cells on soft surfaces had less bundled stress fibers and lower traction forces on individual pillars at the cell-surface interface, whereas cells on stiff substrates formed ventral stress fibers and had higher traction forces on individual pillars. When ACTN was knocked down we observed a decrease in the stiffness measured by AFM (Fig. 4) and increased local actin density, traction stress, and ordering of stress fibers on soft substrates (Fig. 3). Overexpression of ACTN resulted in the opposite phenotype; cell stiffness increased such that the critical stiffness was no longer accessible and cells remained unpolarized. Consistent with this, lowering cell stiffness with intermediate concentrations of blebbistatin while not completely abolishing contractile activity was sufficient to induce cytoskeletal order on soft substrates. This mechanosensing mechanism requires active processes and, indeed, in the regime of very low active stress with large doses of blebbistatin ($\zeta_0 \rightarrow 0$), the phenotypes of soft and stiff substrates converge, as intuitively expected and correctly predicted by the model. Furthermore, this mechanism requires cells to form adhesions and exert traction stresses; when this is not possible, for example in a talin knockout (41, 42), cells cannot form ventral stress fibers or polarize on any substrate.

Importantly, Eq. **1** together with Eq. **2** predict that actin ordering S depends on E_s and E_c only via E_s/E_c. The main prediction of the model was found to be in good agreement with experimental observations (Fig. 5*A*). Note that f determined in Eq. **2** depends in principle on the cell Poisson's ratio, which was assumed constant in Fig. 5*A*; large variation of the Poisson's ratio have however been reported and could lead to important effects (43). It should be noted that while cell stiffness measured by AFM and in the model both correlated with ACTN concentration and myosin II activity, the exact measured values were different from those used in the model due to the complex nature of cellular mechanical properties including heterogeneous, anisotropic, and unknown Poisson's ratio of actin structures.

Microtubule Organization Exhibits Similar Dependence on Substrate and Cell Stiffness. In our experiments, the polarization of the actin cytoskeleton and cell polarization appeared to go hand-in-hand with stress fibers spanning the long axis of the cell body. As the actin cytoskeleton is not the sole determinant of cell polarity, we questioned whether nematic organization of actin also affected the organization of the microtubule cytoskeleton. Disrupting microtubules with nocodazole resulted in decreased nematic ordering of the cytoskeleton (*SI Appendix*, Fig. S2 *E* and *F*), which we attributed to an increase in contractility from released GEF-H1 (44). To test this, we seeded cells onto soft and stiff pillar substrates and performed immunostaining to visualize the microtubules and quantified the order parameter in the same manner as actin. We found that the microtubule cytoskeleton became more linearly organized on stiff substrates compared to soft substrates (*SI Appendix*, Fig. S10) and furthermore followed the same trend as the actin cytoskeleton of soft and stiff substrates as ACTN was knocked down or overexpressed, or myosin II was inhibited. This provided evidence that the breaking of symmetry and polarization of the actin cytoskeleton also resulted in downstream cellular adaptations to substrate rigidity.

Discussion

We propose a model for the organization of the actin cytoskeleton at the cell scale on substrates with differing rigidities (Fig. 5*B*), which is controlled by the relative cell-to-substrate stiffness E_s/E_c. Control cells had differential organization on soft and stiff substrates, whereby they were more polarized on stiff substrates. When the actin network stiffness was increased by overexpressing ACTN, E_s/E_c decreased and cells had reduced polarization on both soft and stiff substrates. Conversely, lowering the cytoskeletal stiffness by either knocking down ACTN or inhibiting myosin II

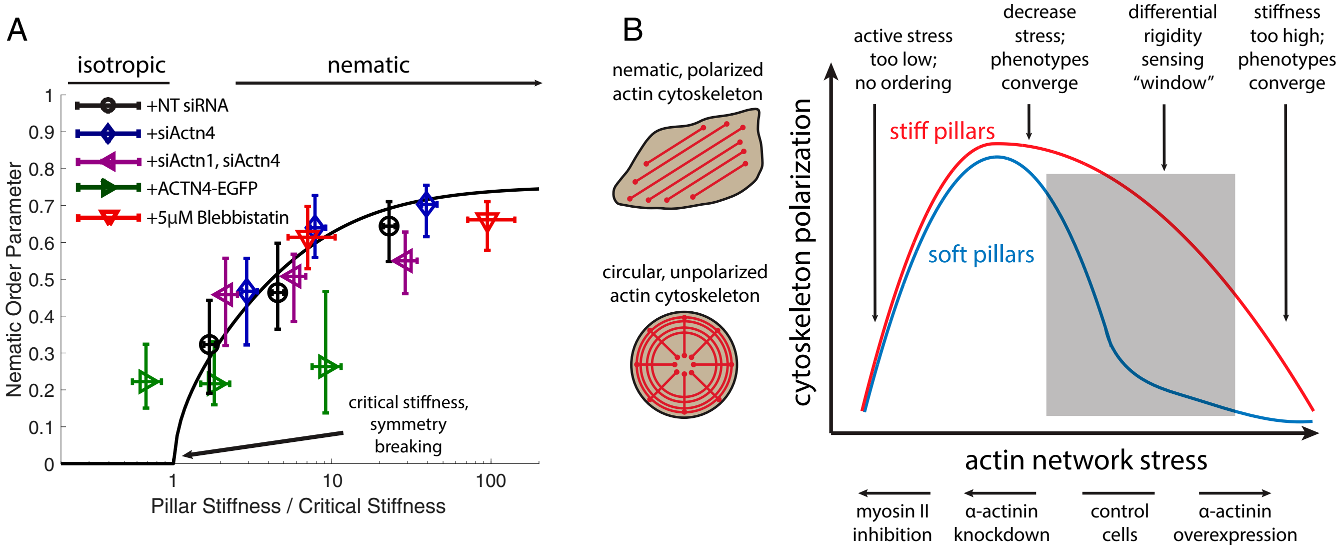

Fig. 5. Actin cytoskeleton stiffness governs substrate stiffness-dependent nematic organization of actin. (*A*) Plot of nematic order parameter versus pillar stiffness normalized to critical stiffness for various cell treatments. $k^* = 2.4$, 1.4, 1.9, 6.0, and 0.58 nN/μm for NT siRNA treatment, ACTN4 knockdown, pan-ACTN knockdown, ACTN4-EGFP overexpression, and 5 μM blebbistatin, respectively. Solid line indicates solution to Eqs. **1** and **2**. with $C = 1$, $\rho_0 = 1$, $(\gamma/\omega)^{1/2} = 1.4$, $\rho_c = 1.1$, and $2\chi\zeta = 0.28$. Data shown is reproduced from Figs. 2 and 3, vertical error bars indicate the interquartile range and horizontal error bars indicate the 95% confidence interval from fitting k* to Eqs. **1** and **2**. (*B*) Cartoon showing the nematic organization of actomyosin network on stiff (red) and soft (blue) substrates as a function of actin network stress, which may be perturbed by changing the levels of ACTN cross-linking or inhibiting myosin II. Areas in gray indicate where differential adaptation to substrate rigidity occurs, and outside of this region the phenotype on soft and stiff substrates converge.

increased E_s/E_c and the cytoskeleton had enhanced polarization on soft substrates. Thus, a simple explanation is that softening the cell cytoskeleton, whether by reducing the myosin contractility or depleting cross-linkers, will promote cell polarization on soft substrates whereby stiffer cells will require higher substrate rigidity to break symmetry, and differential cytoskeletal adaptation between soft and stiff substrates exists at a specific "window" of actomyosin network stress for a given cell type outside of which the phenotype converges. Further, the cellular traction forces on soft distributed more evenly throughout the cell body, but on stiff condensed onto fewer pillars; this configuration favors cell polarization since the traction force symmetry is inherently broken and a subset of adhesions are reinforced. Remarkably, this proposed mechanism depends only on cell scale properties of the actin cytoskeleton (active stress and stiffness) and the antagonistic relationship between passive intracellular elasticity and myosin II-mediated active stress. Thus, it is expected to be independent of the specific molecular players governing these properties (45) but rather depends on the emergent rheological properties after integrating the roles of many proteins. As such, rigidity sensing cannot be solely controlled at the scale of focal adhesions but requires a contractile component that generates force. Molecular factors that are important at both the adhesion and cell scales include 1) increased stability of focal adhesions on stiff substrates induced by local contractile forces at focal adhesions (17), 2) extracellular matrix ligand presented and specific integrin subunits activated by the cell (30), 3) enhanced formin-mediated actin polymerization under tension (46), 4) enhanced cofilin-mediated severing of actin in highly cross-linked systems (47), 5) competitive binding between ACTN and tropomyosin (35, 36), and 6) cross-linker binding kinetics, which for ACTN4 includes catch-bond behavior (48, 49) and is mutated in focal segmental glomerulosclerosis to increase its binding affinity to actin (50).

A normal cell differentiates between soft and stiff substrates; in our model this is only possible when the intracellular stress is within a specific window, thus some natural regulation of contractility and cross-linking is required for a normal cell to function properly in a given environment. If a cell is perturbed such that the rheological properties of the cytoskeleton are affected, then our model predicts that it would lose sensitivity to substrate rigidity. This has been shown to be the case in many transformed cell lines that are unable to sense rigidity due to lack of local contractility events (51), and furthermore, transformed cells are often measured as softer than normal cells (52). Other studies have also shown that reducing cytoskeletal tension will increase cell proliferation and spread area on soft surfaces while having a smaller effect on hard surfaces (52–54). Along this line, ACTN4 knockdown fibroblasts proliferate in very soft environments (17). In conclusion, our study provides a physical mechanism by which the intrinsic rheological properties of the cytoskeleton couple with force-sensing adhesions to govern its adaptive response to substrate rigidity and cell-scale mechanosensing, which further dictate the behavior of higher-order cellular functions.

Materials and Methods

Further information regarding experimental procedures are detailed in the accompanying *SI Appendix*.

Preparation of Pillar Substrates. PDMS micropillars were fabricated as previously described (55). Briefly, 10:1 PDMS ratio was mixed and poured into deep-reactive ion etched silicon molds, degassed, and cured at 80 °C for 2 h. Human plasma fibronectin (Roche) was conjugated with Atto-647N using a protein labeling kit (catalog no. 76508, Sigma-Aldrich). Blank PDMS stamps were incubated in 50 μg/mL pure fibronectin and 1 μg/mL conjugated fibronectin in Dulbecco's phosphate-buffered saline (DPBS) at room temperature for at least 90 min, washed once with Milli-Q water, and dried in N_2 stream. Pillars were treated in UV-ozone for 15 min (UV Ozone ProCleaner Plus, BioForce Nanosciences), and fibronectin was transferred to the pillar tops by microcontact printing, incubated with 0.2% Pluronic F-127 for 1 h, and washed multiple times with DPBS and left at 4° until ready to use. The pillar spring constant k was determined as in Schoen et al. (56); the Young's modulus of PDMS was assumed to be 2 MPa and $\nu = 0.5$. Pillars were arranged in a close-packed hexagonal lattice with 4 μm center-to-center distance and the dimensions of pillars (imaged by scanning electron microscopy) were: d = 2.1 μm with h = 4.1 μm (k = 55 nN/μm), d = 2.0 μm with h = 7.0 μm (k = 11 nN/μm), and d = 1.8 μm with h = 8.6 μm (k = 4.1 nN/μm).

Calculation of the Order Parameter. The order parameter was calculated using a custom-built MATLAB program. Briefly, the local orientation θ of actin and coherence was determined at each pixel from the structure tensor of the image (Peter Kovesi, MATLAB and Octave Functions for Computer Vision and Image Processing, Available from: https://www.peterkovesi.com/matlabfns). Pixels with coherence less than 0.08 were discarded. The order parameter is $S = \langle\cos(2|\theta - \theta_{avg}|)\rangle$, where θ_{avg} is the average angle of actin. All averages were weighted by the fluorescence intensity. The radial order parameter was calculated by as $S_\theta = \langle\cos(2|\theta - \theta_{COM}|)\rangle$, where θ_{COM} is the angle of the vector between a given position to the center of mass of the cell. Cell aspect ratio and area were calculated using the built-in MATLAB function regionprops of a binary-masked actin image.

Atomic Force Microscopy. Plastic Petri dishes (TPP) were incubated in 10 μg/mL fibronectin in PBS at 4 °C overnight on a 60-rpm shaker. Cells were seeded and allowed to adhere at least 3 h. AFM nanoindentation experiments were performed using a Nanowizard 4 (JPK Instruments) in Quantitative Imaging mode with a 37 °C Petri dish heater. The imaging buffer was Leibovitz's L-15 medium supplemented with 10% fetal bovine serum and 1× penicillin-streptomycin. PFQNM-LC-A-CAL cantilevers (Bruker) were used; the nominal tip radius was 70 nm (confirmed by scanning electron microscopy), the spring constant for each probe was provided by the manufacturer, and the optical lever sensitivity was determined by the thermal tuning method in liquid. Force-indentation curves were collected with 100 μm/s probe velocity, 400 pN trigger force, and variable indentation-retraction distance (scanning frequency) over a $(60 \times 60)\ \mu m^2$ area with 128 × 128 pixel resolution. Curves were fit in a linearization scheme (57) for the elastic modulus $E/(1 - \upsilon^2)$ by the Hertz model modified for a thin sample adhered to an infinitely rigid substrate (58) using a custom-built MATLAB program. The height at each indentation was determined from the contact point relative to the substrate, and the Poission's ratio was assumed to be 0.5 for rigid substrate correction only.

Data Availability. All data are available in the manuscript and *SI Appendix*.

Further information regarding experimental procedures are detailed in the accompanying *SI Appendix*.

ACKNOWLEDGMENTS. This work was supported by the Mechanobiology Institute (MBI), European Research Council Grant No. CoG-617233, Labex Who Am I? Grant ANR-11-LABX-0071, Université de Paris IdEx Grant ANR-18-IDEX-0001, the National University of Singapore-Université de Paris program, the Agence Nationale de la Recherche ("POLCAM" Grant No. ANR-17-CE13-0013 and "CODECIDE" Grant No. ANR-17-CE-13-0022), Ligue Contre le Cancer (Equipe labellisée, R.-M.M. and B.L.), and Singapore Ministry of Education Academic Research Fund Tier 3 Grant MOE2016-T3-1-002 and Tier 2 Grant MOE2016-T2-1-096 (to M.P.S.). We thank MBI wet laboratory and microscopy core support, Sree Vaishnavi and Mohammed Ashraf (MBI microfabrication core), and Ratna Prasuna Vogirala and Paramasivam Kathirvel (MBI protein expression core). We thank Alexander Bershadsky, Ronen Zaidel-Bar, Hu Shiqiong, Meenubharathi Natarajan, Shreyansh Jain, Delphine Delacour, Anh Phuong Le, Brenda Mui Hoon Nai, and all other members of the M.P.S. and B.L. laboratories for helpful discussions, reagents, and assistance.

1. D. Choquet, D. P. Felsenfeld, M. P. Sheetz, Extracellular matrix rigidity causes strengthening of integrin-cytoskeleton linkages. *Cell* **88**, 39–48 (1997).
2. D. Riveline *et al*., Focal contacts as mechanosensors: Externally applied local mechanical force induces growth of focal contacts by an mDia1-dependent and ROCK-independent mechanism. *J. Cell Biol.* **153**, 1175–1186 (2001).
3. C. M. Lo, H. B. Wang, M. Dembo, Y. L. Wang, Cell movement is guided by the rigidity of the substrate. *Biophys. J.* **79**, 144–152 (2000).
4. A. J. Engler, S. Sen, H. L. Sweeney, D. E. Discher, Matrix elasticity directs stem cell lineage specification. *Cell* **126**, 677–689 (2006).
5. M. Théry *et al*., Anisotropy of cell adhesive microenvironment governs cell internal organization and orientation of polarity. *Proc. Natl. Acad. Sci. U.S.A.* **103**, 19771–19776 (2006).
6. T. Chen *et al*., Large-scale curvature sensing by directional actin flow drives cellular migration mode switching. *Nat. Phys.* **15**, 393–402 (2019).

7. T. Iskratsch, H. Wolfenson, M. P. Sheetz, Appreciating force and shape—The rise of mechanotransduction in cell biology. *Nat. Rev. Mol. Cell Biol.* **15**, 825–833 (2014).
8. A. Engler *et al*., Substrate compliance versus ligand density in cell on gel responses. *Biophys. J.* **86**, 617–628 (2004).
9. A. Saez, A. Buguin, P. Silberzan, B. Ladoux, Is the mechanical activity of epithelial cells controlled by deformations or forces? *Biophys. J.* **89**, L52–L54 (2005).
10. L. Trichet *et al*., Evidence of a large-scale mechanosensing mechanism for cellular adaptation to substrate stiffness. *Proc. Natl. Acad. Sci. U.S.A.* **109**, 6933–6938 (2012).
11. T. Yeung *et al*., Effects of substrate stiffness on cell morphology, cytoskeletal structure, and adhesion. *Cell Motil Cytoskeleton* **60**, 24–34 (2005).
12. M. Prager-Khoutorsky *et al*., Fibroblast polarization is a matrix-rigidity-dependent process controlled by focal adhesion mechanosensing. *Nat. Cell Biol.* **13**, 1457–1465 (2011).
13. M. Gupta *et al*., Adaptive rheology and ordering of cell cytoskeleton govern matrix rigidity sensing. *Nat. Commun.* **6**, 7525 (2015).
14. S. V. Plotnikov, A. M. Pasapera, B. Sabass, C. M. Waterman, Force fluctuations within focal adhesions mediate ECM-rigidity sensing to guide directed cell migration. *Cell* **151**, 1513–1527 (2012).
15. H. Wolfenson *et al*., Tropomyosin controls sarcomere-like contractions for rigidity sensing and suppressing growth on soft matrices. *Nat. Cell Biol.* **18**, 33–42 (2016).
16. B. Yang *et al*., Mechanosensing controlled directly by tyrosine kinases. *Nano Lett.* **16**, 5951–5961 (2016).
17. G. Meacci *et al*., α-Actinin links extracellular matrix rigidity-sensing contractile units with periodic cell-edge retractions. *Mol. Biol. Cell* **27**, 3471–3479 (2016).
18. M. Sheetz, A tale of two states: Normal and transformed, with and without rigidity sensing. *Annu. Rev. Cell Dev. Biol.* **35**, 169–190 (2019).
19. J. Étienne *et al*., Cells as liquid motors: Mechanosensitivity emerges from collective dynamics of actomyosin cortex. *Proc. Natl. Acad. Sci. U.S.A.* **112**, 2740–2745 (2015).
20. D. Mitrossilis *et al*., Single-cell response to stiffness exhibits muscle-like behavior. *Proc. Natl. Acad. Sci. U.S.A.* **106**, 18243–18248 (2009).
21. K. D. Webster, A. Crow, D. A. Fletcher, An AFM-based stiffness clamp for dynamic control of rigidity. *PLoS One* **6**, e17807 (2011).
22. Y. H. Tee *et al*., Cellular chirality arising from the self-organization of the actin cytoskeleton. *Nat. Cell Biol.* **17**, 445–457 (2015).
23. M. L. Gardel *et al*., Elastic behavior of cross-linked and bundled actin networks. *Science* **304**, 1301–1305 (2004).
24. D. H. Wachsstock, W. H. Schwartz, T. D. Pollard, Affinity of alpha-actinin for actin determines the structure and mechanical properties of actin filament gels. *Biophys. J.* **65**, 205–214 (1993).
25. D. H. Wachsstock, W. H. Schwarz, T. D. Pollard, Cross-linker dynamics determine the mechanical properties of actin gels. *Biophys. J.* **66**, 801–809 (1994).
26. M. L. Gardel *et al*., Prestressed F-actin networks cross-linked by hinged filamins replicate mechanical properties of cells. *Proc. Natl. Acad. Sci. U.S.A.* **103**, 1762–1767 (2006).
27. H. Ennomani *et al*., Architecture and connectivity govern actin network contractility. *Curr. Biol.* **26**, 616–626 (2016).
28. F. Senger *et al*., Spatial integration of mechanical forces by α-actinin establishes actin network symmetry. *J. Cell Sci.* **132**, jcs236604 (2019).
29. S. Hu *et al*., Long-range self-organization of cytoskeletal myosin II filament stacks. *Nat. Cell Biol.* **19**, 133–141 (2017).
30. P. Roca-Cusachs *et al*., Integrin-dependent force transmission to the extracellular matrix by α-actinin triggers adhesion maturation. *Proc. Natl. Acad. Sci. U.S.A.* **110**, E1361–E1370 (2013).
31. H. W. Johnson, M. J. Schell, Neuronal IP3 3-kinase is an F-actin-bundling protein: Role in dendritic targeting and regulation of spine morphology. *Mol. Biol. Cell* **20**, 5166–5180 (2009).
32. P. W. Oakes, Y. Beckham, J. Stricker, M. L. Gardel, Tension is required but not sufficient for focal adhesion maturation without a stress fiber template. *J. Cell Biol.* **196**, 363–374 (2012).
33. M. Gupta *et al*., Cell shape and substrate stiffness drive actin-based cell polarity. *Phys. Rev. E* **99**, 12412 (2019).
34. N. Wang *et al*., Cell prestress. I. Stiffness and prestress are closely associated in adherent contractile cells. *Am. J. Physiol. Cell Physiol.* **282**, C606–C616 (2002).
35. S. Hu *et al*., Reciprocal regulation of actomyosin organization and contractility in nonmuscle cells by tropomyosins and alpha-actinins. *Mol. Biol. Cell* **30**, 2025–2036 (2019).
36. J. P. Kemp Jr., W. M. Brieher, The actin filament bundling protein α-actinin-4 actually suppresses actin stress fibers by permitting actin turnover. *J. Biol. Chem.* **293**, 14520–14533 (2018).
37. K. S. Foley, P. W. Young, An analysis of splicing, actin-binding properties, heterodimerization and molecular interactions of the non-muscle α-actinins. *Biochem. J.* **452**, 477–488 (2013).
38. H. Shao, J. H. Wang, M. R. Pollak, A. Wells, α-actinin-4 is essential for maintaining the spreading, motility and contractility of fibroblasts. *PLoS One* **5**, e13921 (2010).
39. N. Schierbaum, J. Rheinlaender, T. E. Schäffer, Combined atomic force microscopy (AFM) and traction force microscopy (TFM) reveals a correlation between viscoelastic material properties and contractile prestress of living cells. *Soft Matter* **15**, 1721–1729 (2019).
40. P. G. de Gennes, J. Prost, *The Physics of Liquid Crystals*, (Clarendon Press, 1993).
41. Y. Wang *et al*., Label-free single-molecule quantification of rapamycin-induced FKBP-FRB dimerization for direct control of cellular mechanotransduction. *Nano Lett.* **19**, 7514–7525 (2019).
42. X. Zhang *et al*., Talin depletion reveals independence of initial cell spreading from integrin activation and traction. *Nat. Cell Biol.* **10**, 1062–1068 (2008).
43. M. S. Hall *et al*., Fibrous nonlinear elasticity enables positive mechanical feedback between cells and ECMs. *Proc. Natl. Acad. Sci. U.S.A.* **113**, 14043–14048 (2016).
44. Y.-C. Chang, P. Nalbant, J. Birkenfeld, Z.-F. Chang, G. M. Bokoch, GEF-H1 couples nocodazole-induced microtubule disassembly to cell contractility via RhoA. *Mol. Biol. Cell* **19**, 2147–2153 (2008).
45. S. R. Naganathan *et al*., Morphogenetic degeneracies in the actomyosin cortex. *eLife* **7**, e37677 (2018).
46. M. Yu *et al*., mDia1 senses both force and torque during F-actin filament polymerization. *Nat. Commun.* **8**, 1650 (2017).
47. H. Wioland, A. Jegou, G. Romet-Lemonne, Torsional stress generated by ADF/cofilin on cross-linked actin filaments boosts their severing. *Proc. Natl. Acad. Sci. U.S.A.* **116**, 2595–2602 (2019).
48. E. S. Schiffhauer *et al*., Mechanoaccumulative elements of the mammalian actin cytoskeleton. *Curr. Biol.* **26**, 1473–1479 (2016).
49. N. Y. Yao *et al*., Stress-enhanced gelation: A dynamic nonlinearity of elasticity. *Phys. Rev. Lett.* **110**, 18103 (2013).
50. A. J. Ehrlicher *et al*., Alpha-actinin binding kinetics modulate cellular dynamics and force generation. *Proc. Natl. Acad. Sci. U.S.A.* **112**, 6619–6624 (2015).
51. B. Yang *et al*., Stopping transformed cancer cell growth by rigidity sensing. *Nat. Mater.* **19**, 239–250 (2020).
52. H. H. Lin *et al*., Mechanical phenotype of cancer cells: Cell softening and loss of stiffness sensing. *Oncotarget* **6**, 20946–20958 (2015).
53. D. J. McGrail, Q. M. Kieu, J. A. Iandoli, M. R. Dawson, Actomyosin tension as a determinant of metastatic cancer mechanical tropism. *Phys. Biol.* **12**, 26001 (2015).
54. J. D. Mih, A. Marinkovic, F. Liu, A. S. Sharif, D. J. Tschumperlin, Matrix stiffness reverses the effect of actomyosin tension on cell proliferation. *J. Cell Sci.* **125**, 5974–5983 (2012).
55. M. Gupta *et al*., Micropillar substrates: A tool for studying cell mechanobiology. *Methods Cell Biol.* **125**, 289–308 (2015).
56. I. Schoen, W. Hu, E. Klotzsch, V. Vogel, Probing cellular traction forces by micropillar arrays: Contribution of substrate warping to pillar deflection. *Nano Lett.* **10**, 1823–1830 (2010).
57. J. R. Staunton, B. L. Doss, S. Lindsay, R. Ros, Correlating confocal microscopy and atomic force indentation reveals metastatic cancer cells stiffen during invasion into collagen I matrices. *Sci. Rep.* **6**, 19686 (2016).
58. P. D. Garcia, R. Garcia, Determination of the elastic moduli of a single cell cultured on a rigid support by force microscopy. *Biophys. J.* **114**, 2923–2932 (2018).